Available online at www.sciencedirect.com
ScienceDirect
International Journal of Thermal Sciences 47 (2008) 620–632
International Journal of Thermal Sciences
www.elsevier.com/locate/ijts

Numerical investigation of mixed convective heat transfer for unsteady turbulent flow over heated blocks in a horizontal channel

Shiang-Wuu Perng [a], Horng-Wen Wu [b,*]

[a] *Department of Accounting Information, Kun Shan University of Technology, No. 949, Da Wan Rd., Yung-Kang City, Tainan Hsien, 710, Taiwan, Republic of China*
[b] *Department of Systems and Naval Mechatronic Engineering, National Cheng Kung University, Tainan, Taiwan, Republic of China*

Received 21 June 2006; received in revised form 3 January 2007; accepted 2 April 2007

Available online 31 May 2007

Abstract

The turbulent flow field and heat transfer enhancement of mixed convection in a horizontal block-heated channel was investigated, using the Large Eddy Simulation (LES) and SIMPLE-C method coupled with preconditioned conjugate gradient methods. A rectangular turbulator was mounted in the channel to enhance heat transfer by means of an internal flow modification induced by vortex shedding in this study. The width-to-height ratio of turbulator was changed (0.25, 0.5 and 1.0) with a constant Reynolds number (5000) under various Grashof numbers (0–5.0E+8) for the purpose of investigating the heat transfer performance. The results indicate that the turbulator mounted in cross-flow above an upstream block can effectively enhance the heat transfer performance of mixed convection in the horizontal channel.

Keywords: LES; Heat transfer enhancement; Mixed convection; Heated blocks

1. Introduction

In the last decade, convective cooling of electronic components mounted on the circuit boards has been the subject of a large number of scientific papers [1–5], because an electronic device has become more compact and hence densely packaged in response to the demands for cost savings and higher performance. Improvements in cooling methods are required in order to avoid unacceptable temperature rises. The air-cooling of an array of rectangular sources is of particular interest. Mixed convection has recently received considerable attention because the heat transfer is important within electronic components.

The technology of enhancing heat transfer in the forced convection regime by means of vortex generators was discussed in several papers. Sparrow et al. [6] experimentally investigated the effect of implemented barriers in arrays of rectangular modules and reported significant improvement in the heat transfer coefficient of the module in the second row downstream of the barrier. Chou and Lee [7] conducted an experimental work on the possibility of reducing flow non-uniformities in LSI packages by vortex generating from a rectangular plate on the top of a downstream chip. Myrum et al. [8] have conducted a series of experiments on dealing vortex generators (circular rods) induced enhancement of heat transfer from ribbed ducts in which different generator configurations were investigated by changing rod diameter, rod–rib spacing and rod–rod spacing.

Although many papers have been conducted on enhancement techniques for forced convection, there are few studies on natural convection. One of enhancement techniques is to modify flow pattern through vortex-shedding employing little on mixed convection enhancement. Wu and Perng [9] presented a numerical study on the heat transfer enhancement of laminar flow through vortex shedding from an inclined plate in a channel containing heated blocks. The enhancement technique investigated here is to use a rectangular turbulator with various width-to-height ratios to generate vortex shedding in a horizontal block-heated channel. Examining the efficiency of the enhancement technique for mixed convection in the turbulent flow is a motivation to us from practical consideration. The present research is a numerical study of mixed convection enhancement in the turbulent flow. The purpose of this study is to

* Corresponding author.
E-mail address: z7708033@email.ncku.edu.tw (H.-W. Wu).

1290-0729/$ – see front matter
doi:10.1016/j.ijthermalsci.2007.04.003

Nomenclature

B	width of the turbulator
C_K	SGS model variable in LES ($C_K = 0.094$)
C_P	pressure coefficient ($\int P\,\mathrm{d}A'/\int \mathrm{d}A'$)
$[C_P]$	time-mean pressure coefficient ($\int C_P\,\mathrm{d}t/\int \mathrm{d}t$)
C_S	Smagorinsky constant
D	hydraulic diameter of channel ($D = 2H$)
$\mathrm{d}A$	surface area increment along the block
$\mathrm{d}A'$	surface area increment along y-axis direction for the turbulator
E_{SGS}	dimensionless subgrid-scale kinetic energy
f_S	frequency of the vortex shedding
f_μ	Van Driest wall damping function ($[1-\exp(-y_n^+/25)^3]^{1/2}$)
G	grid filter function
Gr	Grashof number ($g\beta q H^4/k\nu^2$)
h	height of the block, height of the turbulator
H	channel height
l	dimensionless characteristic length scale
L	channel length
n	normal vector
Nu	Nusselt number ($-\frac{1}{\theta_w}\frac{\partial\theta}{\partial n}$)
$[Nu]$	time-mean Nusselt number ($\int Nu\,\mathrm{d}t/\int \mathrm{d}t$)
$\langle Nu\rangle$	surface-mean Nusselt number ($\int Nu\,\mathrm{d}A/\int \mathrm{d}A$)
P	dimensionless static pressure ($P_S/\rho u_\infty^2$)
P_S	static pressure
P^*	summation of $\bar{P}$ and $\frac{2}{3}E_{\mathrm{SGS}}$
P^{n+1}	dimensionless static pressure for next time step
Pr	Prandtl number (ν/λ)
Pr_T	turbulent Prandtl number
q	heat flux at wall boundary
R	computational domain
Re	Reynolds number based on channel height ($u_\infty H/\nu$)
Re_D	Reynolds number based on twice channel height ($u_\infty D/\nu$)
Re_{eff}	effective Reynolds number
Re_{SGS}	SGS Reynolds number
St	Strouhal number ($St = h\cdot f_S/u_\infty$)
S_{ij}	strain rate tensor of the flow field ($S_{ij} = \frac{1}{2}(\frac{\partial u_i}{\partial x_j}+\frac{\partial u_j}{\partial x_i})$)
$\lvert\bar{S}\rvert$	mean strain ($\lvert\bar{S}\rvert = \sqrt{2\bar{S}_{ij}\bar{S}_{ij}}$)
S_Φ	source term for variable
T^*	temperature
T_∞	uniform inlet temperature
t	dimensionless time ($t^*/(H/u_\infty)$)
t^*	time
Δt	dimensionless time interval
u, v	dimensionless velocity components ($u = u^*/u_\infty, v = v^*/u_\infty$)
u_∞	uniform inlet velocity
u_τ	friction velocity ($u_\tau \equiv \sqrt{\frac{\tau_W}{\rho}}$)
u^*, v^*	velocity components
w	width of the block
x, y	dimensionless x^*, y^* coordinates ($x = x^*/H$, $y = y^*/H$)
x^*, y^*	physical coordinates
x_i	Cartesian coordinates ($i = 1$ for x-coordinate; $i = 2$ for y-coordinate)
y_w	near-wall distance
y_n^+	dimensionless distance from the wall ($y_n^+ \equiv \frac{y_w u_\tau}{\nu}$)

Greek symbols

$\bar{\Delta}$	grid filter width
Φ	general dependent flow variable
Φ'	subgrid-scale component of Φ
Γ_Φ	diffusion coefficient
λ	thermal diffusivity
ν	laminar kinematic viscosity
ρ	density
τ_W	wall shear stress
θ	dimensionless temperature ($(T^*-T_\infty^*)/(qH/k)$)
ξ	natural coordinate in computational domain
ζ	dimensionless distance along ribbed wall in Lockett's reference [26]

Superscript

–	spatial grid filter indication

Subscript

i, j	indication of components
w	indication of wall boundary

quantify the influence of width-to-height ratio of the rectangular turbulator on heat transfer enhancement under various Grashof numbers.

The Reynolds-averaged simulations require a fine grid to resolve the regions of rapid variations. Given the complexity of the Reynolds-averaged simulations, a Large Eddy Simulation (LES) might actually be simpler, shorter in execution and more accurate. In the Reynolds-averaged simulations the length scales of the turbulence are usually much larger than the grid spacing. The Reynolds-averaged simulations only reveal unsteady motions of scales larger than the model's turbulence scale. Besides, the eddy viscosity is obtained from the length scale of the smallest eddy in the turbulent models. Therefore, the volume-average filtered Navier–Stokes equations are fairly insensitive to the turbulent models in a Large Eddy Simulation (LES) [10]. The turbulent, vortex-shedding flow a long square cylinder, which is two-dimensional in the mean, is simulated by Large Eddy Simulation (LES). When the mean flow is two-dimensional, it is common for engineering problems to perform two-dimensional computation, because CPU time is then reduced greatly in comparison with three-dimensional computation [11].

In this paper, the SIMPLE-C method [12] and LES [13] are employed in investigating the fluid modification by means of vortex shedding generated by a rectangular turbulator and its effect on heat transfer enhancement of mixed convection occurring in heated blocks. The first order implicit method [14] is implemented for discretizing the transient term and Extended Linear Upwind Differencing (ELUD) method (third-order scheme) [15] for discretizing the convection terms to avoid severe oscillations. Also, iterative solution methods based on the preconditioned conjugate gradient method [16,17] were incorporated into the solving process with second-order time advancement.

The SIMPLE-C method coupling with the above discretization techniques generally requires less computer storage and computation time than the conventional SIMPLE method. The results of this study may be of interest to engineers attempting to develop thermal control of electronic devices and to researchers interested in the turbulent flow-modification aspects of heat transfer enhancement of mixed convection in a horizontal channel.

2. Mathematical formulation

The two-dimensional flow geometries are shown in Fig. 1 in which those are installed with and without a turbulator under investigation. The unsteady, turbulent, incompressible flow is used to investigate the mixed convection heat transfer over heated blocks mounted on one side of the horizontal channel in this paper. The calculation of the thermal turbulent flow field with the Large Eddy Simulation (LES) requires obtaining the solution of the governing equations.

In LES the flow variables are decomposed into a large-scale component, denoted by an overbar, and a subgrid-scale component. The large-scale component is defined by the following operation:

$$\overline{\Phi}(x_i,t)=\int_R G(x_i-\xi)\Phi(\xi)\,\mathrm{d}\xi,\quad \Phi=\overline{\Phi}+\Phi' \tag{1}$$

where the integral is extended over the entire domain R, and G is the grid filter function. The length associated with G is the grid filter width $\bar{\Delta}$.

The dimensionless transport equations representing the conservation of mass, momentum and thermal energy are cast into a general form of time-dependent and two-dimensional Cartesian coordinates, and the dimensionless governing transport equations are in terms of being filtered by a simple volume-averaged box filter under the Boussineq approximation [18] as follows:

$$\frac{\partial\bar{\Phi}}{\partial t}+\frac{\partial}{\partial x}\left(\bar{u}\bar{\Phi}\right)+\frac{\partial}{\partial y}\left(\bar{v}\bar{\Phi}\right)$$

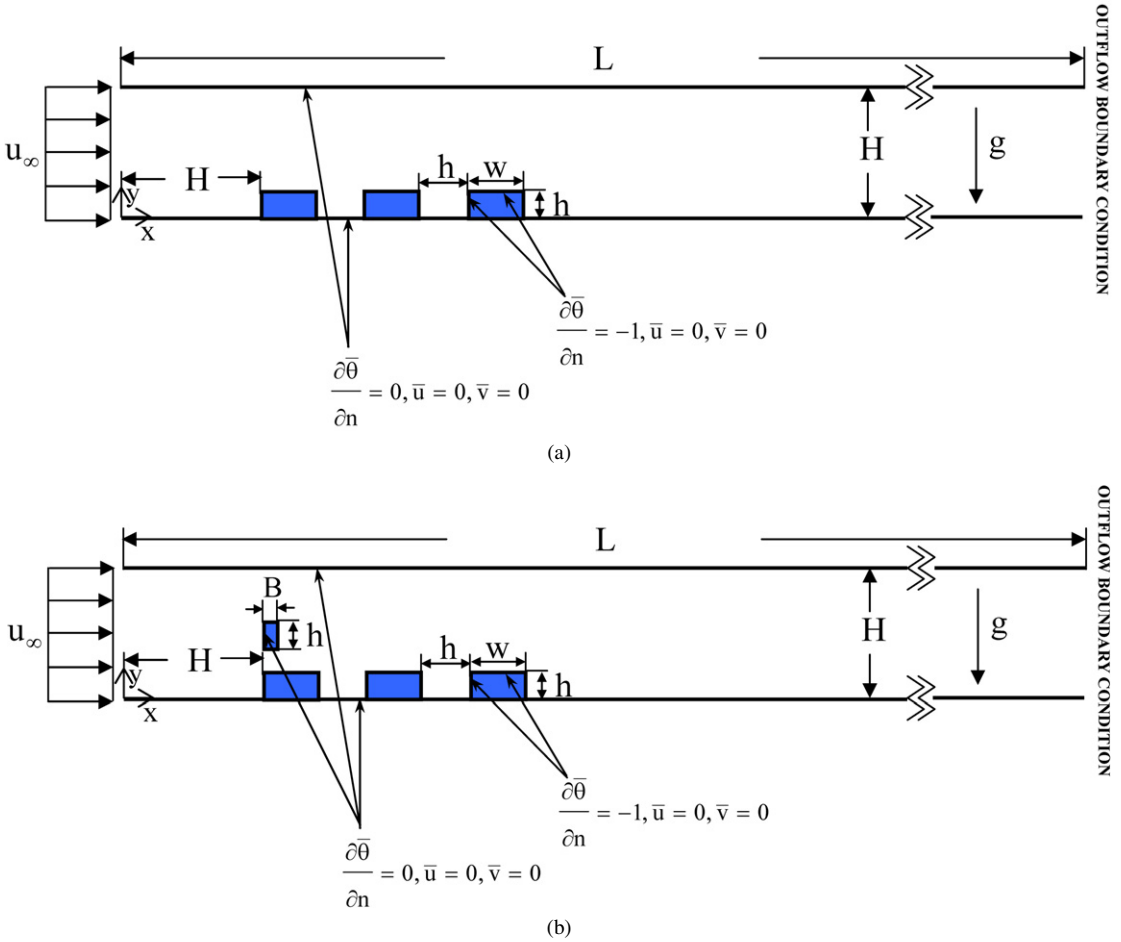

Fig. 1. The geometries considered here: (a) without a rectangular turbulator, (b) with a rectangular turbulator above the first block.

Table 1
Definition of Φ, Γ_Φ and S_Φ

Φ	Γ_Φ	S_Φ
1	0	0
u	$\frac{1}{Re_{\text{eff}}}$	$-\frac{\partial P^*}{\partial x}+\frac{\partial}{\partial y}(\frac{1}{Re_{\text{eff}}}\frac{\partial \bar{v}}{\partial y})+\frac{\partial}{\partial x}(\frac{1}{Re_{\text{eff}}}\frac{\partial \bar{u}}{\partial y})$
v	$\frac{1}{Re_{\text{eff}}}$	$-\frac{\partial P^*}{\partial y}+\frac{\partial}{\partial y}(\frac{1}{Re_{\text{eff}}}\frac{\partial \bar{v}}{\partial y})+\frac{\partial}{\partial x}(\frac{1}{Re_{\text{eff}}}\frac{\partial \bar{u}}{\partial y})+\frac{Gr}{Re^2}\bar{\theta}$
θ	$\frac{1}{PrRe}+\frac{1}{Pr_T Re_{\text{SGS}}}$	0

Note:

$$\frac{1}{Re_{\text{eff}}}=\frac{1}{Re}+\frac{1}{Re_{\text{SGS}}},\quad P^*=\overline{P}+\frac{2}{3}E_{\text{SGS}},\quad E_{\text{SGS}}=\left(\frac{1}{C_K\bar{\Delta}}\cdot\frac{1}{Re_{\text{SGS}}}\right)^2$$

$C_K=0.094$ [19], $Pr_T=0.9$ [20].

$$=\frac{\partial}{\partial x}\left(\Gamma_\Phi\frac{\partial\bar{\Phi}}{\partial x}\right)+\frac{\partial}{\partial y}\left(\Gamma_\Phi\frac{\partial\bar{\Phi}}{\partial y}\right)+S_\Phi(x,y) \tag{2}$$

where $\bar{\Phi}$ represents one of the following entities: 1, u, v, or θ, in which the dependent dimensionless variables are velocity components u, v, and temperature θ. Also, t is dimensionless time, and Γ_Φ and S_Φ stand for the corresponding effective diffusion and source term, respectively. The corresponding expressions of Γ_Φ and S_Φ are given in Table 1. In Eq. (2), the notation $\bar{\Phi}=1$ denotes the continuity equation.

In Table 1, Re_{SGS} is the subgrid-scale (SGS) Reynolds number, Re_{eff} is the effective Reynolds number, P is the static pressure, and E_{SGS} is the SGS turbulent kinetic energy.

2.1. Turbulence modeling

Initial runs of the present research revealed that the conventional Smagorinsky model [21] did not generate appropriate levels of eddy viscosity in the complex physical domain. For the reason, the Van Driest wall damping SGS model [22] is used here as follows.

$$\frac{1}{Re_{\text{SGS}}}=l^2\times\sqrt{2\times\tilde{S}_{ij}\tilde{S}_{ij}}$$

$$l=C_S f_\mu\bar{\Delta},\quad f_\mu=\left[1-\exp(-y_n^+/25)^3\right]^{1/2} \tag{3}$$

where l is a dimensionless characteristic length scale of small eddies, C_S is equal to 0.15 [11], f_μ is the Van Driest wall damping function, and $y_n^+\equiv y_w u_\tau/\nu$. The Van Driest wall damping function is used to account for the near wall effect. $\bar{S}_{ij}$ is a dimensionless strain rate tensor of the filtered flow field.

$$\bar{S}_{ij}=\frac{1}{2}\left(\frac{\partial\bar{u}_i}{\partial x_j}+\frac{\partial\bar{u}_j}{\partial x_i}\right),\quad \left|\bar{S}\right|=\left(2\times\bar{S}_{ij}\bar{S}_{ij}\right)^{0.5} \tag{4}$$

2.2. Computational domain, boundary and initial conditions

The computational domains are shown in Fig. 1 for a horizontal block-mounted channel with and without a rectangular turbulator. The geometrical relations for the two channels are set forth: $H/w=2.5$, $L/w=25$, $h/w=0.5$ and different B/h values (0.25, 0.5 and 1). The stream-wise and cross-stream directions are x and y, respectively.

Flow and temperature fields in the near-wall region are matched to the boundary layer models. According to the research of Werner and Wengle [23], we assume that the instantaneous tangential velocity inside the first grid cell is in phase with the instantaneous wall shear stress and that a linear or 1/7 power-law distribution of the instantaneous velocity is used:

$$\frac{\bar{u}}{u_\tau}=y_n^+\quad(\text{when } y_n^+\leqslant 11.81) \tag{5}$$

$$\frac{\bar{u}}{u_\tau}=8.3y_n^{+1/7}\quad(\text{when } y_n^+>11.81) \tag{6}$$

where u_τ is the friction velocity and y_n^+ is the dimensionless distance from the wall. Thermal near-wall boundary conditions coherent with the above instantaneous velocity ones were also implemented. They were based on the universal temperature profiles of Jayatilleke [24] for a Prandtl number of 0.71.

Cases with and without a rectangular turbulator have the same external boundary conditions; uniform inflow with $\bar{u}=1$, $\bar{v}=0$; no-slip boundary conditions $\bar{u}=0$ and $\bar{v}=0$ on the upper and lower channel surfaces; and a standard outflow condition $\partial\bar{u}/\partial x=0$ and $\partial\bar{v}/\partial x=0$ across the outflow plane; $\partial\bar{\theta}/\partial n=-1$ along the heated block surfaces; and $\partial\bar{\theta}/\partial n=0$ along the other surfaces. In the outflow plane, we utilized the "traction free" condition, and the equation of the outflow boundary condition can be used as adopted by Ramaswamy and Jue [25]:

$$\left(\frac{\partial^2}{\partial x^2}+\frac{\partial^2}{\partial y^2}\right)\bar{P}^{n+1}=2\frac{\partial\bar{u}}{\partial x}\frac{\partial\bar{v}}{\partial y}-2\frac{\partial\bar{u}}{\partial y}\frac{\partial\bar{v}}{\partial x} \tag{7}$$

A no-slip surface $\bar{u}=0$ and $\bar{v}=0$ is specified on the rectangular turbulator with zero temperature gradient $\partial\bar{\theta}/\partial n=0$. The initial conditions are $\bar{u}=\bar{v}=\bar{\theta}=0$ in the computational domain for $t=0$. As usual, a physical quantity of great interest is the local Nusselt number Nu along the heated block surfaces, and Nu is calculated by

$$Nu=\frac{-1}{\theta_w}\frac{\partial\theta}{\partial n} \tag{8}$$

where n denotes normal to the heated block surfaces.

3. Numerical methods

The SIMPLE-C algorithm with the control volume approach is adopted to derive the discretized forms of all transport equations arranged into transient, diffusion, convection, and source terms. By adopting an Extended Linear Upwind Differencing (ELUD) for discretizing the convective terms and a first-order accurate fully implicit method for discretizing the transient term, we may derive the fully discretized equations by means of control-volume method. These discretized equations are easily implemented into the SIMPLE-C algorithm.

The iterative solution methods based on the preconditioned conjugate gradient method are incorporated into this code. In this paper, the ICCG method [16] is used for the Poisson pressure correction equation, and the ILUBiCG method [17] is used for the equations of u, v, θ. The dimensionless time step was tested to be set as 0.001 for the calculations of unsteady flow and heat transfer in the block-mounted channel with and without a turbulator. The calculations were terminated when the mass residual is less than 10^{-4} and the solution for nodal velocity components varied less than 10^{-5} between two consecutive iterations.

4. Results and discussion

4.1. Model validation

Using the above description about numerical methods, we investigated the unsteady turbulent flow and mixed convection heat transfer enhancement by placing a rectangular turbulator in a horizontal block-heated channel. Grashof number is considered as 0, 2.5×10^7 and 5×10^8 when Re is kept constant at 5000 and Pr as 0.71. All the calculations have been performed by using a Pentium 4 3.0G PC. After a series of grid independent test runs (150×40; 220×60; 300×80; 360×100, the former is for x-axis and the latter is for y-axis), the mesh (220×60) was chosen for all cases (the sensitivity results as shown in Fig. 2(a)). The time step size is adjusted in this numerical code from stability and accuracy criteria with the initial time step size given as an input. The four time steps 0.0005, 0.001, 0.002, and 0.004 were chosen to test the time step size sensitivity. According to the results in Fig. 2(b), the time increment Δt was set as 0.001 in the calculations of unsteady turbulent flow and heat transfer over heated blocks with and without a rectangular turbulator. In these calculations for the study, about 14,000 time steps were necessary to obtain reasonably reliable statistics. The computation CPU times were about 5 h 47 min 13 s for the case without a turbulator and 7 h 28 min 36 s – 7 h 56 min 23 s for the cases with a turbulator. For proving that the program in this paper can handle turbulent heat transfer and boundary step changes in the channel, we employ the present method to solve the turbulent flow in the ribbed channel employed in the experiments of Lockett [26]. The ratio of square rib height ($h = w$) to channel height (h/H) was 1/9.5, the ratio of channel length to channel height was 8, and Re_D was 30,000 in the ribbed channel for Lockett's experiment. The periodic boundary condition was imposed along the stream-wise direction (x). Besides, the bottom wall has a constant heat flux q on the horizontal wall between ribs and a value $q/3$ on each face of a rib while the top wall was adiabatic for the thermal boundary conditions in the ribbed channel. The mesh size employed for the comparison with references was 96×48 (along x and y directions, respectively). The steady-state solution is obtained by the numerical procedure as mentioned in the previous section. The present predictions for the normalized Nusselt number $Nu/\langle Nu \rangle$ of the bottom wall and rib faces are used to make a comparison with the numerical results calculated by Ciofalo and Collins [27] and the experimental results measured by Lockett as shown in Fig. 3. These curves have the same trend with channel length, and the overall relative difference between the curves is less than 2.15%.

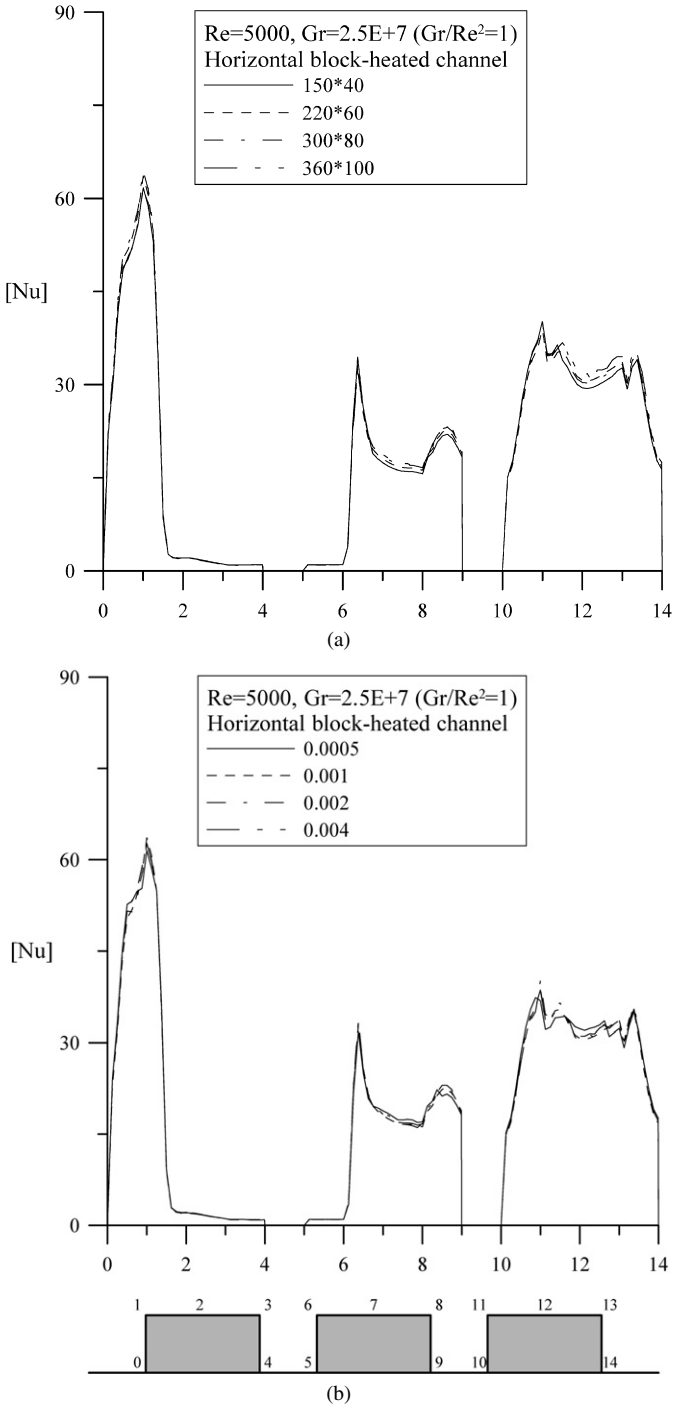

Fig. 2. (a) Grid sensitivity, (b) time step size sensitivity at $Gr/Re^2 = 1$ and $Re = 5000$ for no rectangular turbulator in the horizontal block-heated channel.

4.2. Influence of buoyancy in the absence of a turbulator

In this study, time-mean Nusselt number will be used below for comparing the turbulent heat transfer characteristics between the case with a rectangular turbulator and the case without a turbulator. The time-mean Nusselt number for heated blocks with a rectangular turbulator is calculated in time interval containing several flow cycles of vortex shedding, while the time-mean Nusselt number for the case without a turbulator is calculated in the same time interval. In Fig. 4, the local Nusselt number shows the same characteristic behavior that it increases with an increase in the Gr/Re^2 value. The maximum local Nusselt number for a given block occurs at the front corner while the minimum value occurs at the groove between two blocks. The influence of mixed convection is prominent, especially along the vertical surfaces of the blocks (in the y direction). Similar influence has been presented in an earlier study [28].

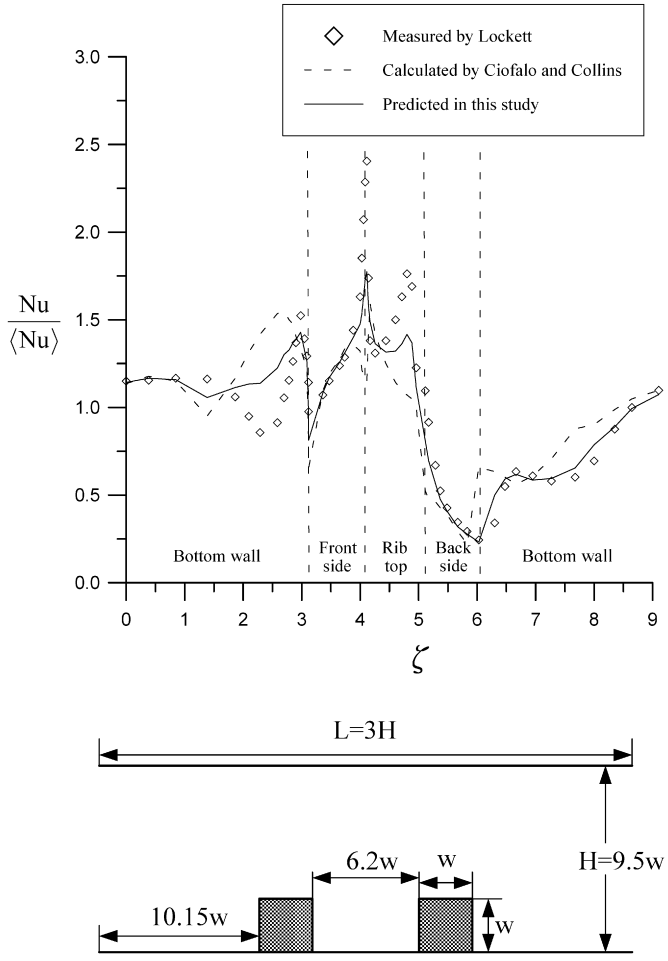

Fig. 3. Comparison of the results between the numerical predictions and Lockett's experiment.

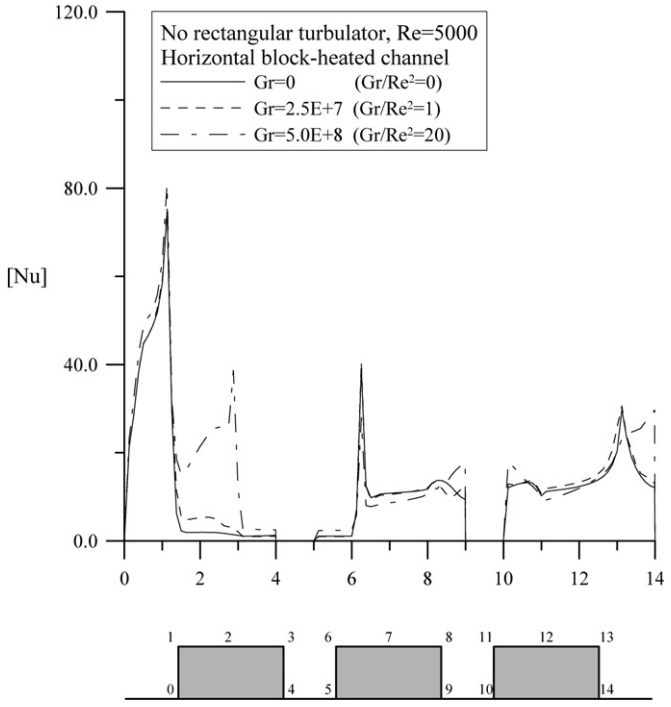

Fig. 4. Time-mean Nusselt number profiles along the block surfaces for Gr/Re^2 values at $Re = 5000$.

For understanding the profiles of Nusselt number further, the streamlines for various Gr values ($Gr = 0$, 2.5E+7, 5E+8) presented in Fig. 5 was utilized to explain these results. The fluid flow around the blocks placed on the lower wall of a channel is very complicated since it is defined by stagnation in front of the first block, separation at the front corner of the first block, a recirculation in the groove between two blocks and another recirculating zone behind the third block (Fig. 5). The curvature of the streamline becomes very large locally at the front cor-

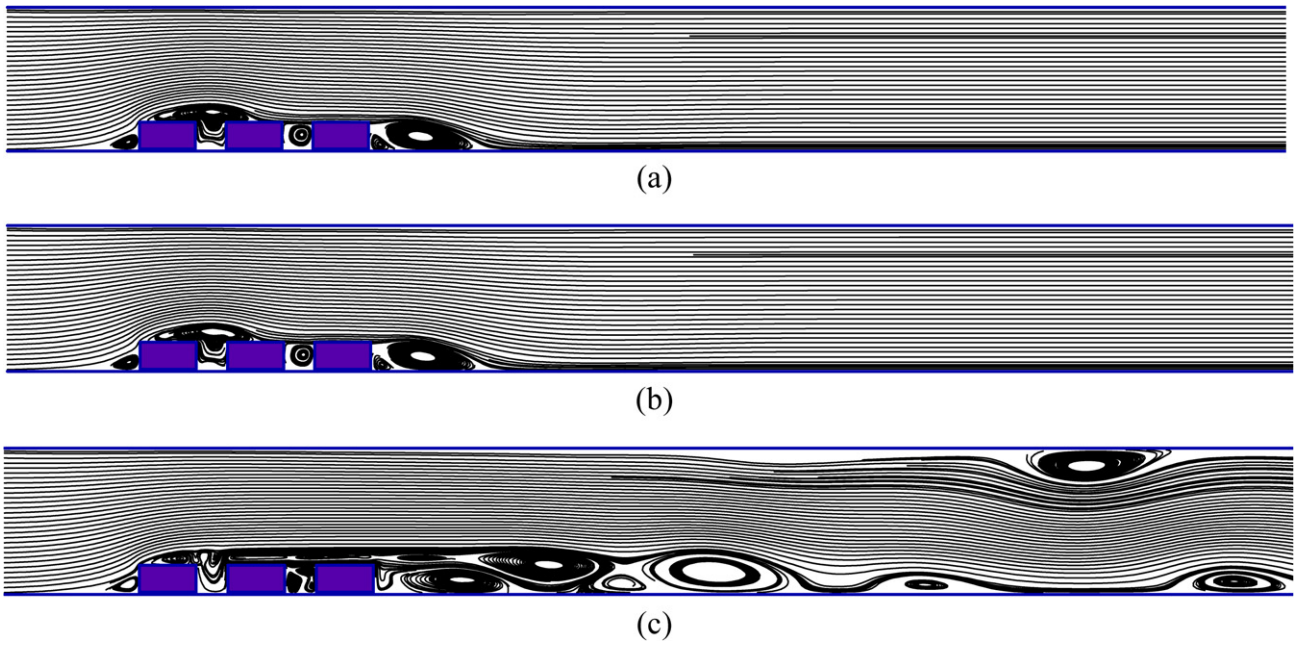

Fig. 5. Stream patterns for $Re = 5000$ at $t = 30$: (a) $Gr/Re^2 = 0$, (b) $Gr/Re^2 = 1$, (c) $Gr/Re^2 = 20$.

ner of a given block; this has a high velocity, so the convection heat transfer is large. Because of separating in front of the first block, there is a small standing vortex around the lower wall of channel. Besides, the strength of the standing vortex is becoming smaller as the Gr/Re^2 value becomes large. A re-circulating zone is formed in the groove between two blocks, so that the heat is transferred poorly from the groove fluid to the mainstream flow. Fig. 5 also shows that there are a bigger clockwise vortex and a smaller counterclockwise vortex in the recirculating zone behind the last block; besides, the re-circulating zone is becoming bigger when Gr/Re^2 increases. Because of upward buoyancy force, the re-circulating zone above the roof around the first two blocks is combined with the vortex between the second and third block, and the re-circulating zone behind the last block to form a bigger re-circulating zone above all blocks when the Gr/Re^2 value is equal to 20. This re-circulating zone above all the blocks makes heat transferred poorly from the horizontal surfaces of the heated block to the mainstream flow, so the distribution of Nusselt number along the surfaces on the roof is smaller obviously than other surfaces in Fig. 4. For $Gr/Re^2 = 20$, the strong buoyant upflow along the vertical surfaces of the blocks (in y direction) facilitates the size of separated eddy and causes other two eddies downstream on the upper and lower walls of a channel. The result of Fig. 5 can provide confirmation to the flow processes.

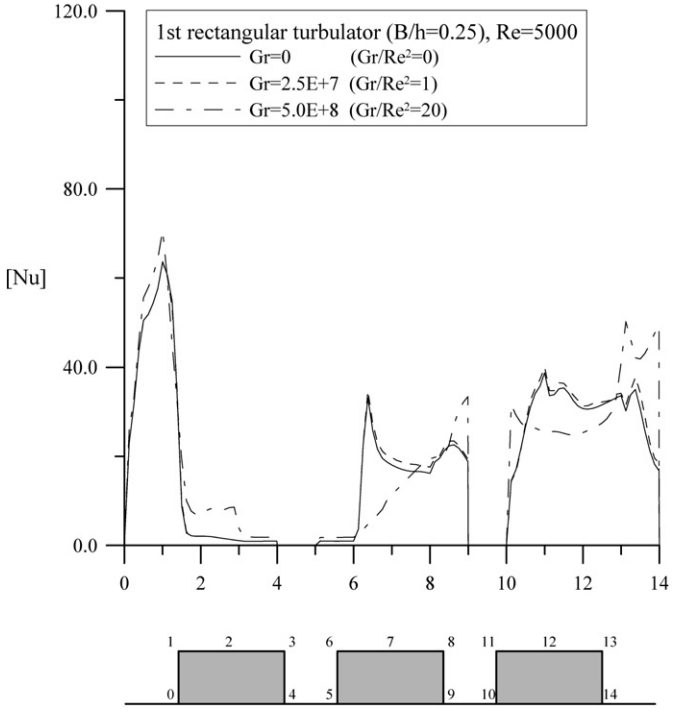

Fig. 6. Effect of Gr/Re^2 values on time-mean Nusselt number profiles installing a rectangular turbulator ($B/h = 0.25$) at $Re = 5000$.

4.3. Influence of buoyancy in the presence of a turbulator

The heat transfer enhancement of a rectangular turbulator installed above the first block is presented in Fig. 6 for three different Gr/Re^2 values at $Re = 5000$. The profile of time-mean Nusselt number along the surfaces of heated blocks is larger than the case without a turbulator as shown in Fig. 4. The flow fields in Fig. 7 can explain this result. Fig. 7 shows the flow fields for the corresponding instantaneous stream patterns each time at the minimum value of pressure coefficient C_P in one vortex-shedding cycle. When $Gr/Re^2 < \mathrm{O}(1)$ (Figs. 7(a) and (b)), wave flows behind the rectangular turbulator pass stronger and faster across these heated blocks, then weaker and slower behind the third block. At $Gr/Re^2 = 20$ (Fig. 7(c)), the buoyancy upflow along the vertical surfaces of the blocks may strengthen the wave flows behind the turbulator, so the wave

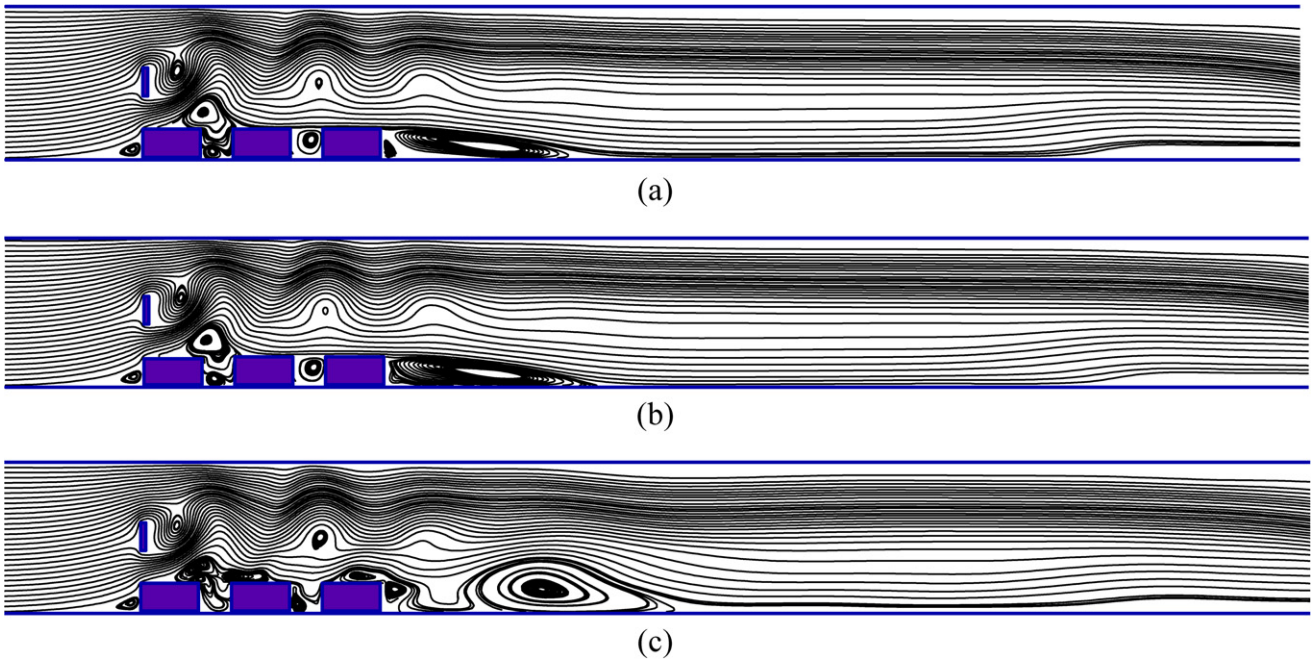

Fig. 7. Stream patterns installing a rectangular turbulator ($B/h = 0.25$) for $Re = 5000$: (a) $Gr/Re^2 = 0$, (b) $Gr/Re^2 = 1$, and (c) $Gr/Re^2 = 20$.

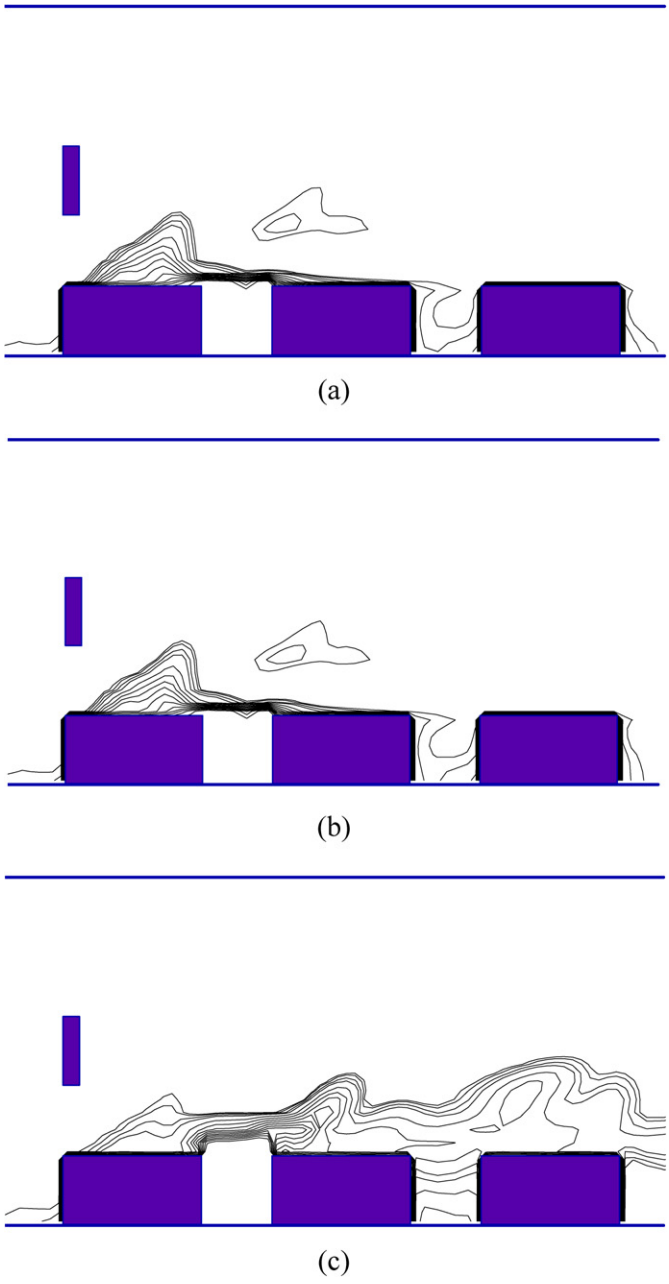

Fig. 8. Local isotherms around blocks for $B/h = 0.25$ at $Re = 5000$: (a) $Gr/Re^2 = 0$, (b) $Gr/Re^2 = 1$, and (c) $Gr/Re^2 = 20$.

motion changes the flow field behind the last block from one recirculating zone into two recirculating zones; the one close to the side surface of the last block is small, and the other one is large. Besides, the smaller re-circulating zone behind the last block also covers the roof of the block, so the distribution of Nusselt number along the surfaces on the roof becomes smaller when Gr/Re^2 equals 20. The strong buoyancy effect uplifts the streamlines from the horizontal surface of the first two blocks to make the re-circulating zone above the roof of the first two blocks move downstream. The moving of the re-circulating zone makes the Nusselt number along the horizontal surface of the second block become smaller. Fig. 8 illustrates the local isothermal distribution around three blocks for $B/h = 0.25$

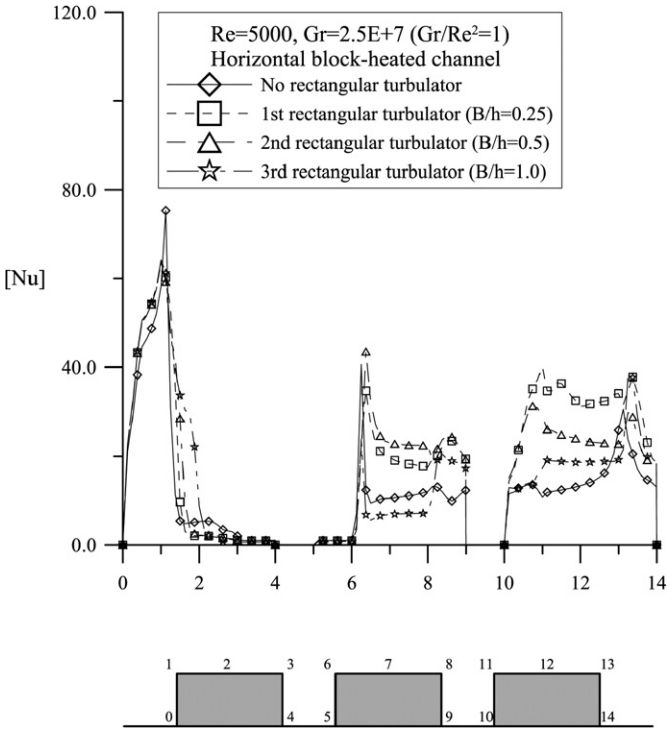

Fig. 9. Influence of width-to-height ratios (B/h) on time-mean Nusselt number profiles compared to no turbulator at $Gr = 2.5\text{E}{+}7$ and $Re = 5000$.

with various Gr/Re^2 values. Closer isothermal lines indicate a higher temperature gradient and accordingly a higher Nusselt number. From Fig. 8, the isothermal lines around the surfaces on the roofs of the last two blocks separate more when Gr/Re^2 equals 20, and then the Nusselt number along these surfaces becomes smaller.

4.4. Influence of the turbulator geometry

For various B/h values the installation of the rectangular turbulator increases the distribution of time-mean Nusselt number along the block surfaces (see Fig. 9). For various B/h values the instantaneous streamlines at the corresponding flow condition are presented in Fig. 10 each time at the minimum of pressure coefficient C_P in one vortex-shedding cycle. For the turbulator with various B/h values, it is evident from Fig. 10 that the separated flow goes along the surfaces and always reattaches on either the upper or the lower surface during a period of the vortex shedding into the wake. Besides, the use of the rectangular turbulator locally accelerates fluid flow through the passageway between the turbulator and the first block but produces different patterns of wave motion induced by vortex shedding. The oscillating fluid motion generated by the turbulator can effectively assist heat transfer along the block surfaces. The improvement in heat transfer for $Gr/Re^2 < \mathrm{O}(1)$ is mainly caused by the oscillations generated by the turbulator. When $Gr/Re^2 > \mathrm{O}(1)$, the heat transfer is improved mainly by a result of the oscillations forcing the mainstream flow to mix with the buoyant upflow along the vertical surfaces of the heated blocks. In Fig. 10, the recirculation above the roof of the first two blocks is moving downstream when the ratio B/h becomes large. The

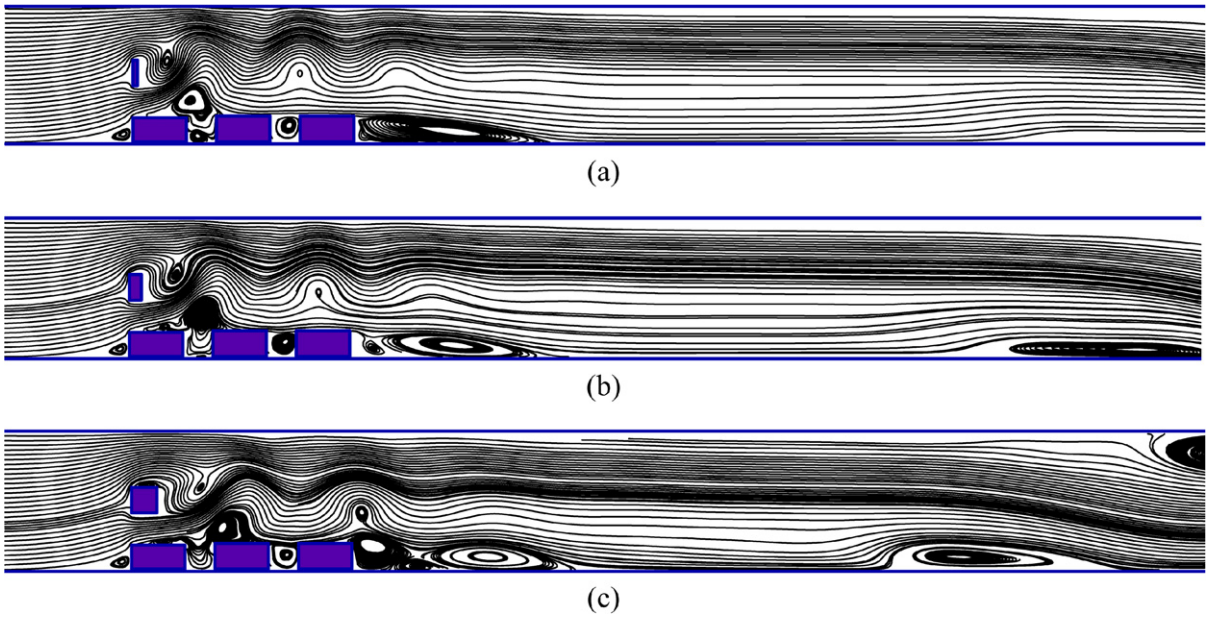

Fig. 10. Stream patterns for various width-to-height ratios at $Gr = 2.5\text{E}{+}7$ and $Re = 5000$: (a) $B/h = 0.25$, (b) $B/h = 0.5$, (c) $B/h = 1$.

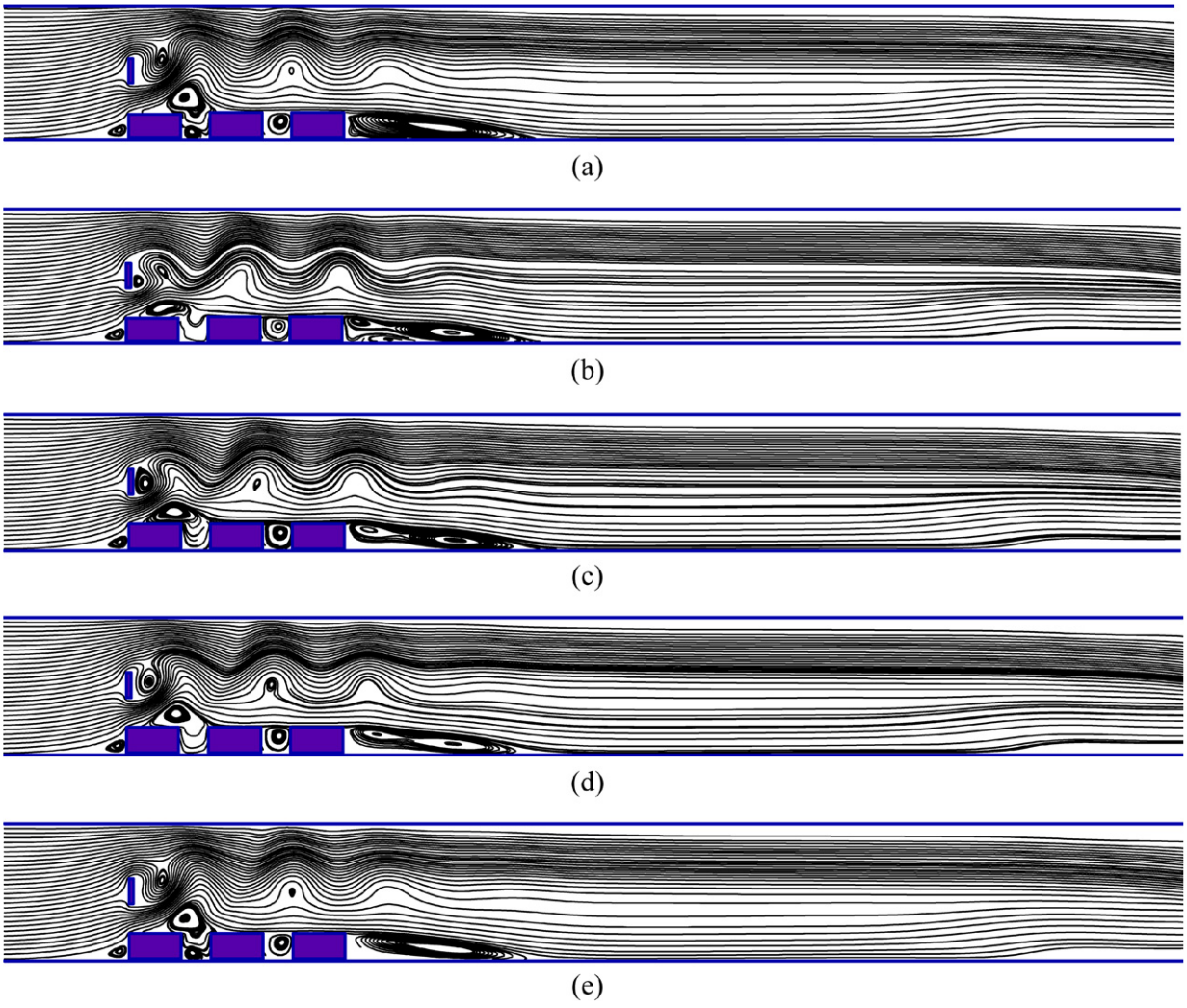

Fig. 11. Sequence of streamlines with a rectangular turbulator ($B/h = 0.25$) during one cycle at (a) $t = 11.704$, (b) $t = 12.404$, (c) $t = 12.614$, (d) $t = 12.81$, (e) $t = 13.048$ for $Gr/Re^2 = 1$ and $Re = 5000$.

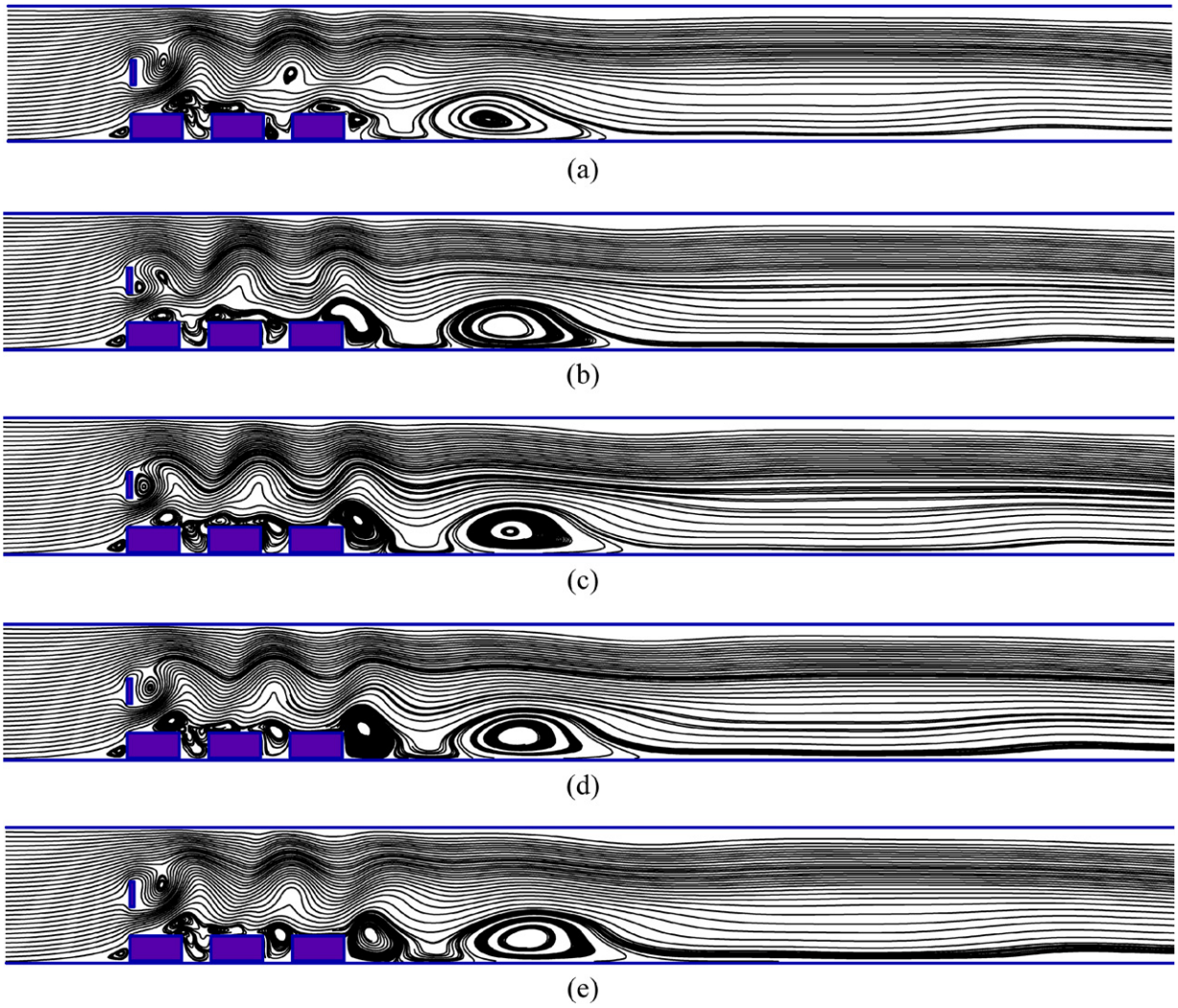

Fig. 12. Sequence of streamlines with a rectangular turbulator ($B/h = 0.25$) during one cycle at (a) $t = 11.788$, (b) $t = 12.517$, (c) $t = 12.745$, (d) $t = 12.96$, (e) $t = 13.174$ for $Gr/Re^2 = 20$ and $Re = 5000$.

recirculation makes heat transferred poorly from the horizontal surfaces of these two heated blocks to the mainstream flow. These results are used to explain that the time-mean Nusselt number is smaller along the horizontal surface of the second block with a turbulator ($B/h = 1$) than without a turbulator. Overall, the wave flows can improve heat transfer along the blocks as shown in Fig. 9.

The time variations of the flow patterns when installing a rectangular turbulator ($B/h = 0.25$) during the flow cycle for $Gr = 2.5\text{E}{+}7$ and $Gr = 5.0\text{E}{+}8$ at $Re = 5000$ are presented in Figs. 11 and 12, respectively. These two figures cover respectively one period of the vortex-shedding process from dimensionless time 11.704 to 13.048 and 11.788 to 13.174. This process demonstrates the event that commences with the shedding of a vortex from the leading tip and ends with the shedding of the next vortex from the same point. For $Gr = 2.5\text{E}{+}7$ and $5.0\text{E}{+}8$, the oscillatory nature of the wake behind the turbulator is similar, but the wave motion for $Gr = 5.0\text{E}{+}8$ is stronger than for $Gr = 2.5\text{E}{+}7$. This motion forms a different pattern of the re-circulating zone behind the last block and the re-circulating zone above the first two blocks. Fig. 13 shows the variation of the pressure coefficient C_P for the rectangular turbulator with $B/h = 0.25$. Because the flow variables are filtered by a simple volume-averaged box filter for LES not by a time-averaged form, the pressure coefficient C_P has unsteady stepwise changes with increasing time. The Strouhal number, or dimensionless vortex-shedding frequency of the flow, is defined by

$$St = h \cdot f_S / u_\infty \tag{9}$$

$St = 0.1488$ is for $Re = 5000$ and $Gr = 2.5\text{E}{+}7$, and $St = 0.1443$ for $Re = 5000$ and $Gr = 5.0\text{E}{+}8$. For investigating the influence of buoyancy effect and width-to-height ratio (B/h) of rectangular turbulator on the pressure coefficient C_P and Strouhal number St, the variations of the time-averaged pressure coefficient $[C_P]$ and St are respectively presented in Fig. 14 and Table 2. In Fig. 14(a), $[C_P]$ is almost the same for different Gr/Re^2 values, in other words, the buoyancy effect on the pressure coefficient C_P is not obvious. From the profiles of $[C_P]$ shown in Fig. 14(b), the pressure coefficient decreases with increasing the width-to-height ratio (B/h) for the rectan-

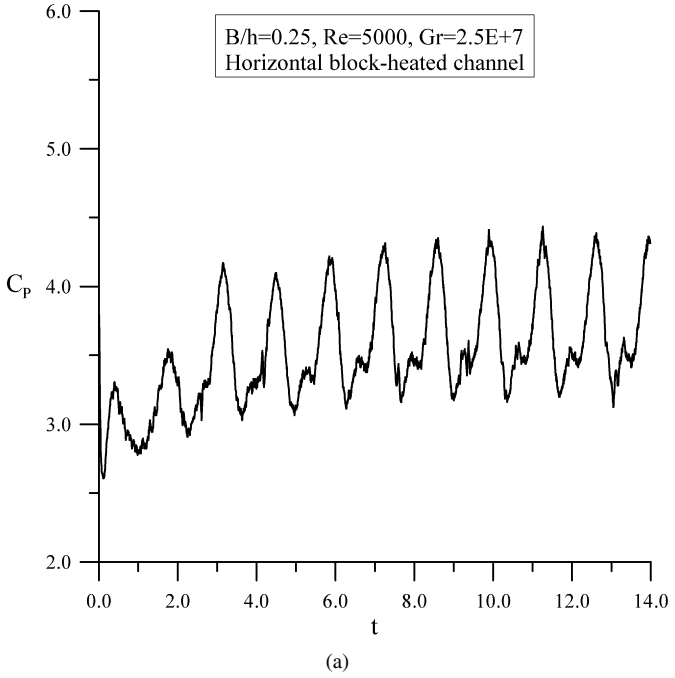

Fig. 13. Pressure coefficient C_P versus dimensionless time for $Re = 5000$ at (a) $Gr = 2.5\text{E}{+}7$ and (b) $Gr = 5.0\text{E}{+}8$.

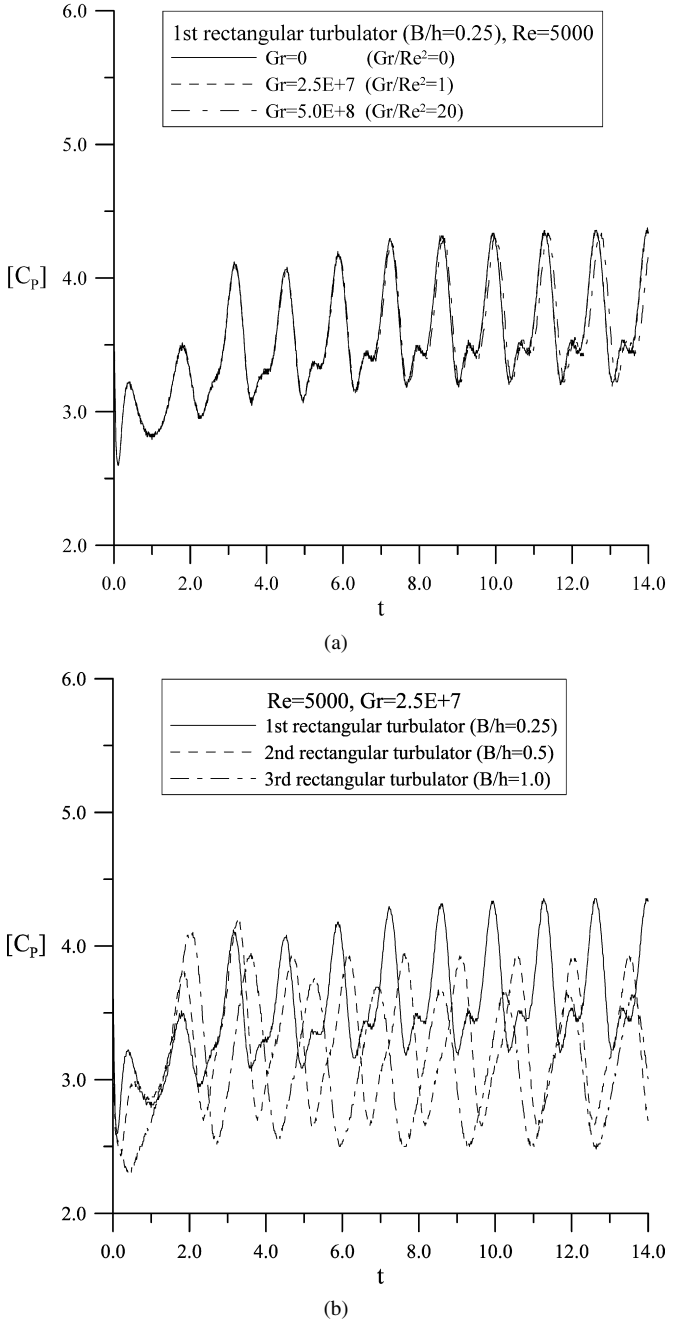

Fig. 14. Influence of various (a) Gr/Re^2 and (b) width-to-height (B/h) values on the time-mean pressure coefficient $[C_P]$ at $Re = 5000$.

gular turbulator. Besides, increasing the B/h value will delay the vortex-shedding process and obtain the phase shift of the vortex shedding. In Table 2, Strouhal number St is almost the same for various Gr values while St decreases slowly with an increase in the width-to-height ratio (B/h). On the other hand, Strouhal number listed in Table 2 is from 0.1189 to 0.1489 for all cases. Similar observations were noted in an earlier study conducted by Okajima [29].

Table 2
Strouhal number St for various B/h and Gr/Re values at $Re = 5000$

	$B/h = 0.25$	$B/h = 0.5$	$B/h = 1.0$
$Gr/Re^2 = 0$ at $Re = 5000$	0.1489	0.1324	0.1200
$Gr/Re^2 = 1$ at $Re = 5000$	0.1488	0.1323	0.1201
$Gr/Re^2 = 20$ at $Re = 5000$	0.1443	0.1309	0.1189

We may investigate the effect of width-to-height ratio of the rectangular turbulator on heat transfer enhancement by means of the values of the average time-mean Nusselt number for the blocks as follows. The average time-mean Nusselt number is calculated by the values of the time-mean Nusselt number on all grid points of the block boundary control volume. The values of average time-mean Nusselt number for the blocks are listed in Table 3 for various B/h values of the turbulator as

Table 3
For three Gr/Re^2 values at $Re = 5000$, values of average time-mean Nusselt number along the block without and with a rectangular plate turbulator

$Gr/Re^2 = 0$ at $Re = 5000$				
Block	No turbulator	$B/h = 0.25$	$B/h = 0.5$	$B/h = 1.0$
1st	15.0493	17.6230 (17.1%)	18.4338 (22.5%)	20.6917 (37.5%)
2nd	9.5333	14.7042 (54.2%)	17.5735 (84.3%)	8.4989 (−10.9%)
3rd	14.2224	29.8091 (109.6%)	24.0215 (68.9%)	19.2724 (35.5%)
Overall	12.9350	20.7121 (60.1%)	20.0096 (54.7%)	16.1543 (24.9%)
$Gr/Re^2 = 1.0$ at $Re = 5000$				
Block	No turbulator	$B/h = 0.25$	$B/h = 0.5$	$B/h = 1.0$
1st	16.2932	17.6278 (8.2%)	18.4400 (13.2%)	20.8709 (28.1%)
2nd	9.4317	15.5732 (65.1%)	17.5795 (86.4%)	8.5160 (−9.7%)
3rd	15.2895	30.9235 (102.3%)	24.0325 (57.2%)	19.2898 (26.2%)
Overall	13.6714	21.3478 (56.3%)	20.0173 (46.4%)	16.2256 (18.7%)
$Gr/Re^2 = 20.0$ at $Re = 5000$				
Block	No turbulator	$B/h = 0.25$	$B/h = 0.5$	$B/h = 1.0$
1st	25.3816	21.2008 (−16.5%)	24.7848 (−2.4%)	30.7225 (21.0%)
2nd	9.2044	12.5996 (36.9%)	16.3567 (77.7%)	6.9457 (−24.5%)
3rd	16.4608	32.0370 (94.6%)	25.3114 (53.8%)	20.9148 (27.1%)
Overall	17.0156	21.9458 (29.0%)	22.1510 (30.2%)	19.5277 (14.8%)

Note: values in parentheses designating the percentage change relative to no rectangular plate turbulator.

well as for no turbulator as the Gr/Re^2 value changes at a fixed value of Re (= 5000). The value of average time-mean Nusselt number for the block increases with increasing Gr for the turbulator as well as for no turbulator except the second block. The minimum value of average time-mean Nusselt number exists at the second block. The value of average time-mean Nusselt number for the whole block increases with an installation of the turbulator compared to no turbulator. The maximum value of average time-mean Nusselt number for the whole block appears at the width-to-height ratio $B/h = 0.25$ with $Gr/Re^2 = 20$. As also shown in parentheses in Table 3, the maximum increase in the overall average time-mean Nusselt number is 60.1% at $B/h = 0.25$ with $Gr/Re^2 = 0$ because of the small time-mean overall average value for no turbulator. For all cases, the maximum increase in the overall average Nu is at $B/h = 0.25$ and the minimum increase is at $B/h = 1.0$; this result is mainly caused by the oscillating wave motion. The wave motion makes the best improvement on heat transfer for $B/h = 0.25$ because the recirculation around the roof between the first and the second block has less influence on the horizontal surfaces of the first and the second blocks. In contrast, for $B/h = 1.0$ the recirculation has obvious influence on the horizontal surface of the second block to get the minimum improvement on heat transfer. The influence of this recirculation mentioned also in Fig. 10 makes heat transferred poor from the horizontal surface of the block to the mainstream flow.

5. Conclusions

A numerical study of the unsteady turbulent flow and mixed convection heat transfer has been systematically performed in a horizontal block-heated channel with and without installing a rectangular turbulator above the first block. The main conclusions emerging from the results and discussion may be summarized as follows.

(1) The results for normalized Nusselt number computed in this paper are in good agreement with available measurements of Lockett.
(2) Installing a rectangular turbulator can effectively improve the turbulent heat transfer characteristics through the modification of the flow pattern.
(3) For $Gr/Re^2 < O(1)$, the buoyancy effect on the turbulent flow and the heat transfer can be neglected. The wave flows induced by vortex shedding behind the rectangular turbulator pass stronger and faster across these three blocks, then weaker and slower behind the last block.
(4) When $Gr/Re^2 = 20$, the buoyancy effect obviously exists along the vertical surfaces of the blocks. The strong buoyant upflow along the vertical surfaces of the blocks interacts with the wave flows and strengthens these flows across the blocks.
(5) For three Gr/Re^2 values, the maximum increase in the overall average time-mean Nusselt number is 60.1% when the width-to-height ratio B/h is 0.25 with $Gr/Re^2 = 0$.

Acknowledgements

The authors gratefully acknowledge the partial financial support of this project by the National Council of the Republic of China.

References

[1] H. Bhowmik, C.P. Tso, K.W. Tou, Analyses of convection heat transfer from discrete heat sources in a vertical rectangular channel, ASME J. Electronic Packaging 127 (2005) 215–222.
[2] M. Nakajima, H. Yanaoka, H. Yoshikawa, T. Ota, Numerical simulation of three-dimensional separated flow and heat transfer around staggered surface-mounted rectangular blocks in a channel, Numer. Heat Transfer Part A 47 (2005) 691–708.
[3] A. Korichi, L. Oufer, Numerical heat transfer in a rectangular channel with mounted obstacles on upper and lower walls, Int. J. Thermal Sci. 44 (2005) 644–655.

[4] Y. Murakami, B.B. Mikic, Parametric optimization of multichanneled heat sinks for VLSI chip cooling, IEEE Trans. Components Packaging Technol. 24 (1) (2001) 2–9.
[5] G. Hetsroni, A. Mosyak, Z. Segal, Nonuniform temperature distribution in electronic devices cooled by flow in parallel microchannels, IEEE Trans. Components Packaging Technol. 24 (1) (2001) 16–23.
[6] E.M. Sparrow, S.B. Vemuri, D.S. Kadle, Enhanced and local heat transfer, pressure drop, and flow visualization, Int. J. Heat Mass Transfer 26 (1983) 689–699.
[7] J.H. Chou, J. Lee, Reducing flow non-uniformities in LSI packages by vortex generator, in: W. Aung (Ed.), Cooling Technology for Electronic Equipment, Hemisphere Publishing Corporation, New York, 1988, pp. 113–124.
[8] T. Myrum, S. Acharya, S. Sinha, X. Qiu, Flow and heat transfer in a ribbed duct with vortex generators, ASME J. Heat Transfer 118 (1996) 294–300.
[9] H.W. Wu, S.W. Perng, Effect of an oblique plate on the heat transfer enhancement of mixed convection over heated blocks in a horizontal channel, Int. J. Heat Mass Transfer 42 (1999) 1217–1235.
[10] C. Fureby, G. Tabor, H.G. Weller, A.D. Gosman, A comparative study of subgrid scale models in homogeneous isotropic turbulence, Phys. Fluids 9 (5) (1997) 1416–1429.
[11] S. Sakamoto, S. Murakami, A. Mochida, Numerical study on flow past 2D square cylinder by large eddy simulation: Comparison between 2D and 3D computations, J. Wind Engrg. Indust. Aerodyn. 50 (1993) 61–68.
[12] J.P. Van Doormaal, G.D. Raithby, Enhancements of the SIMPLE method for predicting incompressible fluid flows, Numer. Heat Transfer 7 (1984) 147–163.
[13] B. Galperin, S. Orszag, Large Eddy Simulation of Complex Engineering and Geophysical Flows, Cambridge Univ. Press, Cambridge, 1993, pp. 231–346.
[14] W. Rodi, Comparison of LES and RANS calculations of the flow around bluff bodies, J. Wind Engrg. Indust. Aerodyn. 69–71 (1997) 55–75.
[15] Y.Y. Tsui, A study of upstream weighted high-order differencing for approximation to flow convection, Int. J. Numer. Methods Fluids 13 (1991) 167–199.
[16] D. Kershaw, The incomplete Cholesky-conjugate gradient method for the iterative solution of systems of linear equations, J. Comp. Phys. 26 (1978) 43–65.
[17] H. Van Der Vorst, BI-CGSTAB: A fast and smoothly converging variant of BI-CG for the solution of nonsymmetric linear system, SIAM J. Sci. Stat. Comput. 13 (2) (1992) 631–644.
[18] S. Habchi, S. Acharya, Laminar mixed convection in a partially blocked vertical channel, Int. J. Heat Mass Transfer 29 (1986) 1711–1722.
[19] A. Yoshizawa, K. Horiuti, Statistically-derived subgrid-scale kinetic energy model for the large-eddy simulation of turbulent flows, J. Phys. Soc. Japan 54 (8) (1985) 2834–2839.
[20] A.W. Verman, B.J. Geurts, J.G.M. Kuerten, P.J. Zandbergen, A finite volume approach to large eddy simulation of compressible, homogeneous isotropic, decaying turbulence, Int. J. Numer. Methods Fluids 15 (1992) 799–816.
[21] J. Smagorinsky, General circulation experiments with the primitive equations, Monthly Weather Rev. 91 (1963) 99–164.
[22] U. Piomelli, High Reynolds number calculations using the dynamic subgrid scale stress model, Phys. Fluids A 5 (6) (1993) 1484–1490.
[23] H. Werner, H. Wengle, Large-eddy simulation of the flow over a square rib in a channel, in: Proc. 7th Symp. Turbulent Shear Flows, Stanford University, 1989, pp. 10.2.1–10.2.6.
[24] C.L.V. Jayatilleke, The influence of Prandtl number and surface roughness on the resistance of the laminar sublayer to momentum and heat transfer, Prog. Heat Mass Transfer 1 (1969) 193–329.
[25] B. Ramaswamy, T.C. Jue, Some recent trends and developments in finite element analytic for incompressible thermal flows, Int. J. Numer. Methods Engrg. 35 (1992) 671–707.
[26] J.F. Lockett, Heat transfer from roughened surfaces using laser interferometers, Ph.D. thesis, Department of Mechanical Engineering, The City University, London, 1987.
[27] M. Ciofalo, M.W. Collins, Large-eddy simulation of turbulent flow and heat transfer in plane and rib-roughened channels, Int. J. Numer. Methods Fluids 15 (1992) 453–489.
[28] S.Y. Kim, H.J. Sung, J.M. Hyun, Mixed convection from multiple-layered boards with cross-streamwise periodic boundary conditions, Int. J. Heat Mass Transfer 35 (11) (1992) 2941–2952.
[29] A. Okajima, Strouhal numbers of rectangular cylinders, J. Fluid Mech. 123 (1982) 379–398.